33rd Annual International Conference of the IEEE EMBS
Boston, Massachusetts USA, August 30 - September 3, 2011

Automated CT Liver Segmentation Using Improved Chan-Vese Model with Global Shape Constrained Energy

Xiuying Wang, Chaojie Zheng, Changyang Li, Yong Yin and David Dagan Feng

Abstract— **In this paper, we propose an automated liver segmentation method to overcome the challenging issues of high degree of variations in liver shape / size and similar density distribution shared by the liver and its surrounding structures. To improve the performance of conventional statistical shape model for liver segmentation, in our method, the signed distance function is utilized so that the landmarks correspondence is not required when performing the principle component analysis. We improve the Chan-Vese model to bind the shape energy and local intensity feature to evolve the surface both globally and locally toward the closest shape driven by the PCA. In our experiments, 20 clinical CT studies were used for training and 25 clinical CT studies were used for validation. Our experimental results demonstrate that our method can achieve accurate and robust liver segmentation from both of low-contrast and high-contrast CT images.**

I. Introduction

COMPUTED tomography (CT) liver segmentation allows for accurate measurement of liver volume and is increasingly used in the treatment and management of diverse liver diseases, for instance, aiding the better localization and evaluation of size and shape of hepatic metastases[1]. Liver segmentation is currently performed manually in clinical practice and it is time-consuming, operator intensive and non-reproducible [2].

A number of early researchers have reported automated or semi-automated segmentation techniques, including intensity range estimation, morphologic operators, and different active models [2-3] to overcome the problems of manual segmentation from high-contrast CT images[4]. These methods mainly based on gradient or intensity analysis may not be able to distinguish the liver from its surrounding organs, which share the similar densities, particularly in low-contrast CT studies. To improve the segmentation, probabilistic atlas based methods were introduced to describe and capture more priori information on the shape, size and position of the liver [5-6]. Accurate mapping of the probabilistic atlas onto the testing CT volumes to determine the performance of segmentation is challenging, due to the variability in liver shapes.

More recently, statistical shape model (SSM) has been introduced to improve CT segmentation. SSM-based segmentation methods use principal component analysis (PCA) to capture and estimate the shape features of the liver [2, 7]. The construction of landmark correspondence for all training datasets [7] is the first step in the majority of SSM based liver segmentation, which is a complicated and time consuming task.

Level-set methods to solve the energy-based active contour minimization problem [8-9], play an important role in various medical image segmentation [10]. The level-set based methods normally take account of the local image features, and thereby it would improve the performance of level-set when the global information on the expected anatomical shape can be included to guide the contour evolution. Leventon et al. [11] and Tsaiet et al. [12] pioneered the use of prior shape knowledge within the level-set framework.

In our paper, we performed PCA on a collection of signed distance functions of the training shape without landmarks required. The group-wise registration was introduced to produce anatomical correspondences among liver training datasets to avoid the bias introduced by pair-wise registration [13]. The shape energy driven by PCA was combined with local image density feature to update the Chan-Vese model to improve the segmentation performance.

II. Methodology

Our algorithm consists of two major parts: shape model training and evolving level-set surface with shape constraint energy.

A. Shape Model Training Phase

The workflow of the shape model training phase is summarized as Fig. 1 that includes liver shape representation and SSM construction.

This research was supported by ARC and PolyU grants.

X. Wang, C. Zheng and C. Li are with the Biomedical and Multimedia Information Technology (BMIT) Research Group, School of Information Technologies, University of Sydney, Australia (e-mails: chli7560@it.usyd.edu.au; xiuying@it.usyd.edu.au).

Y. Yin is with the Department of Radiation Oncology, Shandong Tumor Hospital, Jinan, China (e-mail: yinyongsd@yahoo.com.cn).

David Dagan Feng is with BMIT Research Group, School of IT, University of Sydney, Australia; the CMSP, Department of EIE, Hong Kong Polytechnic University, Hong Kong; and the Med-X Research Institute, Shanghai Jiao Tong University, China.(e-mail: feng@it.usyd.edu.au).

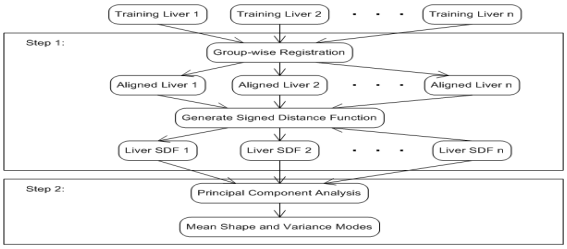

Fig. 1. The framework of shape model training.

1) Liver Shape Representation

A popular and natural approach to represent shapes is via point distribution models where a set of landmarks are used to represent the boundary of the shape. However, as discussed in [12], this approach suffers from problems such as numerical instability, inability to accurately capture high curvature locations, difficulty in handling topological changes and the need for point correspondences.

To overcome these issues, in our algorithm, firstly, the group-wise affine registration is applied to the manually segmented liver training datasets to construct the training shapes alignment and in the mean time to preserve the identity of individual shape. Then we apply SDF [11] to implicitly represent each training shape.

Let Ω be a bounded open subset of R^3. To be consistent with the level-set, as [12], the boundaries of each of the aligned training shapes, denoted by $C \subset \Omega$, are represented as the zero level-set of Lipschitz function $\phi : \Omega \to R$, such that

$$\begin{cases} C = \partial\omega = \{(x,y,z) \in \Omega : \phi(x,y,z) = 0\} \\ inside\ (C) = \omega = \{(x,y,z) \in \Omega : \phi(x,y,z) > 0\} \\ outside\ (C) = \Omega \setminus \overline{\omega} = \{(x,y,z) \in \Omega : \phi(x,y,z) < 0\} \end{cases} \quad (1)$$

By far, for each training liver volume, we generate a SDF representation that is a 3D volume with corresponding SDF values.

2) Statistical Shape Model Construction

Rather than constructing the SSM based on the landmark correspondence in the conventional methods, in our method, the SSM is constructed with the SDF representations of the training shapes.

We form a column vector from each SDF shape representation that is a $N_1 \times N_2 \times M$ volume. Thus, from n training shapes, we construct a vector $X_{SDF}=[x_1 \ \dots \ x_i \ \dots \ x_n]^T$ where x_i is the column vector of SDF shape representation with $N_1 \times N_2 \times M$ elements. PCA is then utilized to capture the variability of the training shapes when constructing SSM.

In PCA, the $n \times n$ covariance matrix S of X_{SDF} is calculated as below:

$$S = \frac{1}{n}\sum_{t=1}^{n} dx_i dx_i^T \quad (2)$$

where $dx_i = x - \bar{x}$ and the mean point $\bar{x}$ in n dimensional space representing the mean shape of training shapes.

Through calculating the eigenvectors and eigenvalues of S, the expected shape x can be derived from the model using:

$$x = \bar{x} + Pb \quad (3)\ [14]$$

where $P = (P_1, P_2 \dots P_t)$ is the matrix representing the first t variation mode, i.e. first t eigenvectors, and $b = (b_1, b_2 \dots b_t)^T$ is the corresponding weight vector of P. In order to keep the shape consistency, b is limited to $-3\sqrt{\lambda} < b < 3\sqrt{\lambda}$, where λ is the eigenvalue of the corresponding eigenvector. The derived x is then transformed back into SDF shape representation and the zero level-set is the boundary of the derived shape.

B. Shape Constrained Surface Evolution Model

1) The Chan-Vese Model

Using level-set, Chan and Vese proposed a general region-based segmentation model [8]. In this model, the segmentation can be achieved via minimizing the following energy function:

$$\begin{aligned} E(c_1, c_2, C) = {} & \mu \cdot Length\ (C) + \upsilon \cdot Area\ (inside\ (C)) \\ & + \lambda_1 \cdot \int_{inside\ (C)} |u_0(x,y,z) - c_1|^2\, dxdy\, dz \\ & + \lambda_2 \cdot \int_{outside\ (C)} |u_0(x,y,z) - c_2|^2\, dxdydz \end{aligned} \quad (4)$$

where C is the active surface , i.e. zero level-set; u_0 is the testing volume; $\mu \geq 0, \upsilon \geq 0, \lambda_1, \lambda_2 > 0$ are the fixed regularizing terms. The model can separate the volume into two partitions with average value c_1, c_2 respectively [8].

However, directly applying the Chan-Vese model to the liver segmentation cannot achieve a robust segmentation result. The expected liver partition may wrongly include other adjacent tissues that share similar densities with liver and the edges among these multiple regions are not easily distinguishable.

To improve this model for a better liver segmentation, we introduce global shape energy derived from SSM into the level-set energy function to regulate the shape of evolving surface for the liver region of interest.

2) Evolving Level-set Surface with Shape Energy

In our algorithm, the shape energy is calculated by minimizing the differences between the surface $u(t)$ and the estimated surface $u_m(t)$ from the SSM at each iteration t using:

$$E_{shape} = \min_t |u(t) - u_m(t)|^2 \quad (5)$$

To obtain the estimated surface u_m from SSM, we update the weights b for equation (3) as defined in [14]:

$$db = P^T dx \quad (6)$$

After introducing this shape energy as defined in (5), the level-set energy function (4) is revised as:

$$\begin{aligned} E_\varepsilon(c_1, c_2, \phi) = {} & \mu \cdot \int_\Omega \delta_\varepsilon(\phi(x,y,z))|\nabla\phi(x,y,z)|dxdydz \\ & + \upsilon \cdot \int_\Omega H_\varepsilon(\phi(x,y,z))dxdydz \\ & + \lambda_1 \cdot \int_\Omega |u_0(x,y,z) - c_1|^2 H_\varepsilon(\phi(x,y,z))dxdydz \\ & + \lambda_2 \cdot \int_\Omega |u_0(x,y,z) - c_2|^2 (1 - H_\varepsilon(\phi(x,y,z)))dxdydz \\ & + \lambda_3 \cdot \int_\Omega |u_0(x,y,z) - u_m(x,y,z)|^2 dxdydz \end{aligned} \quad (7)$$

where $\lambda_3 > 0$ represents the SSM contribution to the surface definition; H is Heaviside function; ϕ is from equation (1) to replace C in equation (4); $\varepsilon \to 0$; c_1 and c_2 are updated during iteration t.

To minimize E_ε with respect to ϕ, the associated Euler-Largrange equation for ϕ is deduced. Parameterizing the descent direction by iteration t, the new speed for level-set equation in $\phi(t,x,y,z)$ is defined as:

$$\frac{\partial\phi}{\partial t} = \delta_\varepsilon(\phi)F = 0$$

$$F = \left[\mu \cdot div\left(\frac{\nabla\phi}{|\nabla\phi|}\right) - \lambda_1(u_0 - c_1)^2 + \lambda_2(u_0 - c_2)^2 - \lambda_3(u_0 - u_m)\right] \quad (8)$$

The process of evolving the surface along the energy minimization direction is performed iteratively until the energy function is converged. In our experiments, to speed up segmentation procedures, the multi-resolution scheme was applied to SSM construction and our revised level-set calculation.

III. Experiments and Discussion

A. Clinical Datasets

Our clinical datasets are comprised of 45 normal studies, including 25 low-contrast CT volumes from GE Discovery LS and 20 high-contrast CT volumes from Philips Brilliance Big Bore. The low-contrast CT images are 512*512 pixels with 16-bit quantization and 4.25mm thickness, and the high-contrast CT images are 512*512 pixels with 16-bit quantization and 3mm thickness.

The liver was manually segmented for all datasets by experienced radiologists. The manually segmented liver volumes were used as the 'ground truth' for validating the accuracy of the automated segmentation. We constructed the shape model from 10 high-contrast and 10 low-contrast CT liver volumes and the remaining 25 datasets were used for validating our segmentation performance.

B. Quantitative Validation

The commonly used metrics for measuring the segmentation quality including the volumetric overlap percentage error (VOPE), the relative volume difference (RVD) [2], and the average square symmetric surface distance (ASD) [2] were employed to quantify the performance of our segmentation method. Table.1 shows that our algorithm was able to segment the liver accurately. It is not surprising that our method worked better on the high-contrast CT volumes when compared to working on the low-contrast CT images, although the accuracy was comparable.

TABLE I Accuracy of Liver Segmentation in High/Low-Contrast CT Images.

	VOPE [%]	RVD [%]	ASD [mm]
15 low-contrast CT datasets	8.9±2.4	3.4±2.7	2.1±0.8
10 high-contrast CT datasets	6.3±2.1	2.3±2.5	1.5±0.2

C. Effect of Shape Energy Constraint

In our experiments, the initial surface for Chan-Vese model was initialized with the mean shape from PCA and placed on the estimated location of the testing liver by using our previous work [15]. To demonstrate the effect of the shape energy on balancing the global and local features in liver segmentation, one example is illustrated as Fig. 2. As shown in Fig.2, simply applying the Chan-Vese model cannot distinguish the exact boundaries among regions with similar density range, and the result was improved after introducing the shape energy to guide surface evolution.

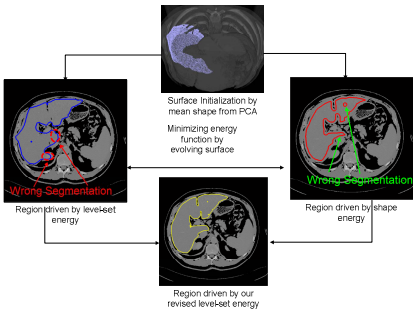

Fig. 2. The illustration of surface evolution driven by different energy functions.

D. Visual Assessment of Segmentation Results

Fig.3 illustrates four groups of experimental segmentation results from our method (delineated in red color) and the manual segmentation (delineated in green color) from high /low-contrast CT volumes for visual assessment.

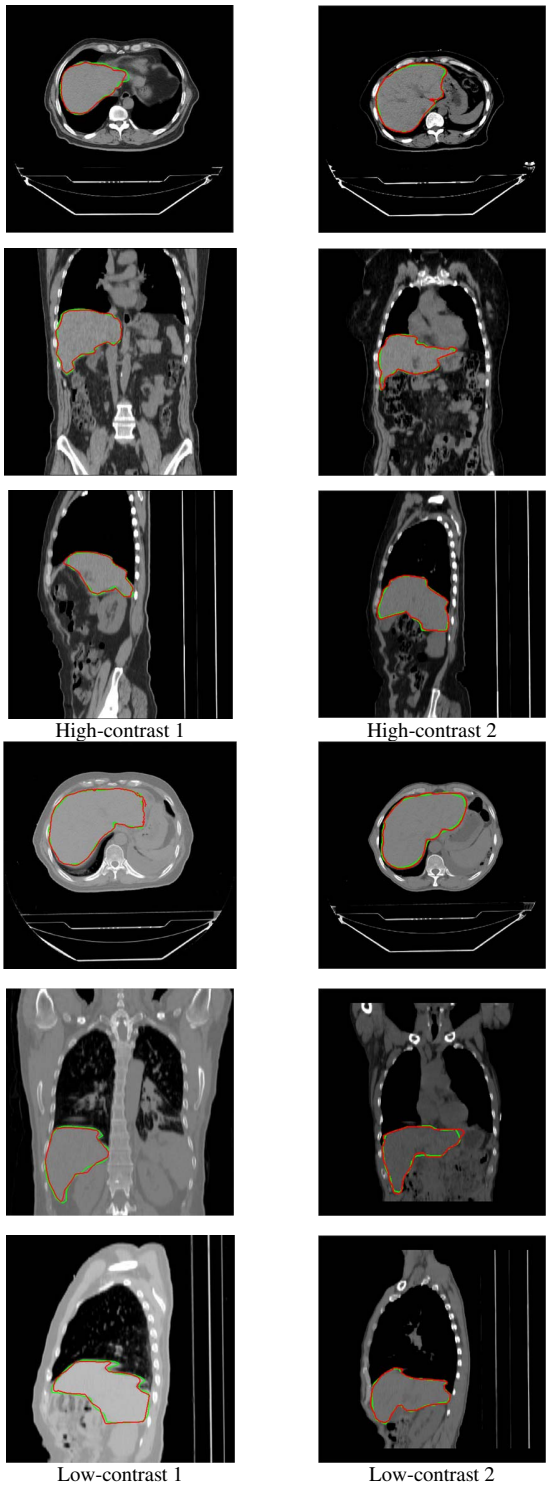

Fig. 3. The transverse, coronal and sagittal views of liver volume segmentation by our method delineated in red and manual segmentation delineated in green for high/low-contrast CT volumes respectively.

IV. Conclusion

We improved the level-set method by taking account into the statistical model information as shape energy. The SDF was applied to represent the implicit surface representation which allowed the PCA construction without the need of landmark correspondence. Our experimental validation on 25 clinical CT volumes demonstrated that our algorithm was robust and accurate to segment the liver from both high-contrast and low-contrast CT images.

References

[1] M. R. Oliva and S. Saini, "Liver cancer imaging: role of CT, MRI, US and PET," *Cancer imaging : the Official Publication of the International Cancer Imaging Society,* vol. 4 Spec No.A, 2004.

[2] T. Heimann, *et al.*, "Comparison and Evaluation of Methods for Liver Segmentation From CT Datasets," *Medical Imaging, IEEE Transactions on,* vol. 28, pp. 1251-1265, 2009.

[3] P. Campadelli and E. Casiraghi, "Liver Segmentation from CT Scans: A Survey," in *Applications of Fuzzy Sets Theory*, 2007, pp. 520-528.

[4] H. B. Ling, *et al.*, "Hierarchical, learning-based automatic liver segmentation," in *Computer Vision and Pattern Recognition(CVPR), IEEE Conference on*, 2008, pp. 1-8.

[5] H. Park, *et al.*, "Construction of an abdominal probabilistic atlas and its application in segmentation," *Medical Imaging, IEEE Transactions on,* vol. 22, pp. 483-492, 2003.

[6] X. Zhou, *et al.*, "Constructing a Probabilistic Model for Automated Liver Region Segmentation Using Non-contrast X-Ray Torso CT images," presented at the Proc. of 9th International Conference for Medical Image Computing and Computer-Assisted Intervention-MICCAI, 2006.

[7] T. Heimann and H. P. Meinzer, "Statistical shape models for 3D medical image segmentation: A review," *Medical Image Analysis,* vol. 13, pp. 543-563, 2009.

[8] T. F. Chan and L. A. Vese, "Active contours without edges," *Image Processing, IEEE Transactions on,* vol. 10, pp. 266-277, 2001.

[9] S. Osher and J. Sethian, "Fronts Propagating with Curvature-Dependent Speed: Algorithms Based on Hamilton-{J}acobi Formulations," *Journal of Computational Physics,* vol. 79, pp. 12-49, 1988.

[10] L. He, *et al.*, "A comparative study of deformable contour methods on medical image segmentation," *Image and Vision Computing,* vol. 26, pp. 141-163, 2008.

[11] M. E. Leventon, *et al.*, "Statistical shape influence in geodesic active contours," in *Computer Vision and Pattern Recognition, 2000. Proceedings. IEEE Conference on*, 2000, pp. 316-323 vol.1.

[12] A. Tsai, *et al.*, "A shape-based approach to the segmentation of medical imagery using level sets," *Medical Imaging, IEEE Transactions on,* vol. 22, pp. 137-154, 2003.

[13] W. R. Crum, *et al.*, "Non-rigid image registration: theory and practice," *The British Journal of Radiology,* vol. 77, pp. 140-153, 2004.

[14] T. F. Cootes, *et al.*, "Active Shape Models-Their Training and Application," *Computer Vision and Image Understanding,* vol. 61, pp. 38-59, 1995.

[15] X. Y. Wang, *et al.*, "Automated liver segmentation for whole-body low-contrast CT images from PET-CT scanners," in *Engineering in Medicine and Biology Society, 2009. EMBC 2009. Annual International Conference of the IEEE*, 2009, pp. 3565-3568.